7734 *Macromolecules* **2010**, *43*, 7734–7743
DOI: 10.1021/ma100925c

Macromolecules
ARTICLE

Self-Assembly in Thin Films of Mixtures of Block Copolymers and Homopolymers Interacting by Hydrogen Bonds

Nathalie Lefèvre,[†,§] Kostas Ch. Daoulas,*[,‡,§] Marcus Müller,[‡] Jean-François Gohy,[†] and Charles-André Fustin*[,†]

[†]*Institute of Condensed Matter and Nanosciences (IMCN), Bio- and Soft Matter (BSMA), Université catholique de Louvain, Place L. Pasteur 1, 1348 Louvain-la-Neuve, Belgium, and* [‡]*Institut für Theoretische Physik, Georg-August-Universität, Friedrich-Hund-Platz, 37077 Göttingen, Germany.* [§] *These authors contributed equally to the present work*

Received April 27, 2010; Revised Manuscript Received June 21, 2010

ABSTRACT: We report on the self-assembling behavior in thin films of mixtures of polystyrene-*block*-poly(ethylene oxide) copolymers (PS-*b*-PEO), having PEO cylindrical microdomains, with poly(acrylic acid) homopolymers (PAA). We study the effect of adding PAA of different molecular weights, specifically interacting with the PEO block by hydrogen bonding, on the thin film characteristics: morphology, microdomain orientation and spacing. It is found that the addition of PAA induces an orientation of the cylindrical microdomains perpendicularly to the film surface. The lattice spacing increases with the amount of PAA added until a transition toward lamellar morphology is observed. This transition occurs at lower PAA content for PAA of small molecular weight. The experiments also reveal that the PAA homopolymer is localized in the center of the PEO microdomains. The trends observed in the experiments were validated by self-consistent field theory calculations using a newly and specifically developed model.

Introduction

Polymer blends are an important class of materials with huge technological interest. Blending is indeed a convenient and efficient route for the development of new materials benefiting from a synergetic effect from the individual components.[1,2] Moreover, the final properties can be easily adjusted by changing the blend composition. A particularly interesting class of blends comprises mixtures of a diblock copolymer with a homopolymer.[1,2] Block copolymers can self-assemble into various morphologies with well-defined periodicities in the range of tens of nanometers giving rise to a variety of applications in materials science or nanotechnology.[3] In this context, blending with a homopolymer provides an interesting method to tune the characteristic dimensions and/or morphology of the self-assembled structures. Such blends can be divided into two categories: (i) blends of an AB copolymer with a homopolymer A (or B), and (ii) blends of an AB copolymer with a homopolymer C which is selectively miscible with the A (or B) block of the copolymer. The phase behavior of the blends belonging to the first category has been studied in details and mainly depends on the ratio between the number of segments of the homopolymer ($N_{A,A}$) and the number of segments of the copolymer block miscible with the homopolymer ($N_{A,AB}$).[4−13] Three regimes can be distinguished: (i) an homogeneous distribution (wet brush regime) of the homopolymer in the A domains of the copolymer for $N_{A,A}/N_{A,AB} < 1$, (ii) a segregation (dry brush regime) of the homopolymer within the A domains for $N_{A,A}/N_{A,AB} \sim 1$, and (iii) a macrophase separation for $N_{A,A}/N_{A,AB} > 1$. For the second category of blends (AB + C), the phase behavior is more complex because it depends, in addition to the $N_C/N_{A,AB}$ ratio, on various parameters.[14−20] The affinity of the homopolymer C for the A block of the copolymer (χ_{AC}) can greatly vary and, in addition, specific interactions between the two sequences, such as hydrogen bonds, can exist, giving usually rise to an increase of miscibility compared to AB + A systems. Moreover, the degree of incompatibility of the homopolymer C with the B block (χ_{AB}) has also to be taken into account. All these parameters strongly influence the interplay between enthalpic and entropic contributions and generate a rich and complex phase behavior.

The vast majority of the studies on blends have been performed in the bulk, but thin mixed films are also of great interest,[9,21−28] especially for nanotechnological applications such as block copolymer lithography or membranes.[29−33] In this context, the cylindrical morphology is particularly desirable since it can be transformed into a dense array of holes. However, there have been few studies on the phase behavior of blends composed of an asymmetric AB copolymer with a homopolymer C in thin films, despite the fact that those systems have a great potential for applications considering the large number of parameters that can be adjusted to tune the desired structure.[9,22,28] Moreover, in the blends studied until now, the homopolymer C has only a weak dipolar interaction with the B block. Here, results on thin films prepared from mixtures of an asymmetric AB copolymer with a homopolymer C, selectively interacting via hydrogen bonds with the B block, are presented. Polystyrene-*block*-poly(ethylene oxide), PS-*b*-PEO, has been chosen as copolymer, and poly(acrylic acid), PAA, as homopolymer. The carboxylic acid group of the PAA can indeed form hydrogen bonds with the ether groups of the PEO. The effect of the molecular weight and the amount of the homopolymer added on the phase behavior of the blends has been studied, in an effort to control the domain spacing and morphology of the thin films, and to understand the impact of the selective interactions between the B and C blocks compared to non, or weakly, interacting systems. To gain further insight into the properties of the morphologies in the PS-*b*-PEO/PAA blends

*Corresponding authors. E-mail:(C.-A.F.) charles-andre.fustin@uclouvain.be; (K.C.D.) daoulas@theorie.physik.uni-goettingen.de.

 Published on Web 08/17/2010

and their dependence on the blend composition and the homopolymer length, the experimental results are compared to self-consistent field theory (SCFT) calculations.

Experimental Section

The polymers were purchased from Polymer Source Inc. Two asymmetric polystyrene-*block*-poly(ethylene oxide) copolymers were used: a PS_{19}-*b*-$PEO_{6.4}$ and a PS_{37}-*b*-$PEO_{6.5}$, where the numbers in subscript represent the number-average molecular weight, M_n, of each block in kg mol^{-1}. Their polydispersity index is equal to 1.05 and 1.06, respectively. Two poly(acrylic acid) homopolymers, PAA, with M_n of 5300 and 20 000 g/mol and polydispersity of 1.1 were selected.

Silicon substrates were cleaned by a piranha solution and carefully rinsed with ultrapure water. Silicon wafers treated with hexamethyldisilazane (HMDS) were also prepared. The substrates cleaned with the piranha solution (Caution!) were dried with a nitrogen flux and placed in a small sealed tank in vapors of HMDS during 60 min. They were then rinsed successively with dichloromethane, methanol and water and sonicated. Solutions of the copolymer-homopolymer blends in tetrahydrofuran (THF), a good solvent for both the copolymer and the homopolymer, were then spin-coated onto these substrates. The spinning speed and/or the solution concentration were used to control the film thickness.

Scanning force microscopy (SFM) images were obtained using a Digital Instruments Nanoscope IV scanning force microscope in tapping mode using NCL type cantilevers (Si, 48 N/m, 330 kHz, Nanosensors).

Self-Consistent Field Theory for PS-*b*-PEO/PAA Blends. *Molecular Model.* A self-consistent field theory (SCFT) approach to the PS-*b*-PEO/PAA blends should account for the conformational dissimilarity of the PS, PEO, and PAA chains as well as the formation of hydrogen bonds between the EO/AA and AA/AA monomer pairs. The blends will be represented as a system of n_s Gaussian chains, where s denotes the polymer molecule species: PS-*b*-PEO or PAA. Following closely the concepts discussed in refs 34−37, we require that the model preserves, for each block or homopolymer species (PS,PEO, and PAA), the molecular volume, v_α, as well as the characteristic size quantified by the average, squared end-to-end distance of the coil, $R_{e(\alpha)}^2$. The subscript, α, stands for the species of the block or the homopolymer: PS, PEO, or PAA. The molecular volume, v_α, can be related to the corresponding monomer number density, $\tilde{\rho}_{o(\alpha)}^{exp}$, in the pure phase of the experimental system and the number of the repeat units of the block or the homopolymer, N_α^{exp}, by:

$$v_\alpha = \frac{N_\alpha^{exp}}{\tilde{\rho}_{o(\alpha)}^{exp}} \tag{1}$$

The stoichiometry of the system is determined taking into account that the weight fraction of the diblocks and homopolymers is φ_s ($\varphi_{PS-PEO} = 1-\varphi_{PAA}$) while their corresponding molecular weight is M_s. Then, the number of diblock and homopolymer chains contained in a mixture of mass M is $n_s = \varphi_s M/M_s$. These chains occupy volumes $V_{PS-PEO} = [v_{PS} + v_{PEO}]n_{PS-PEO}$ and $V_{PAA} = v_{PAA}n_{PAA}$ respectively. If we denote as $V = V_{PS-PEO} + V_{PAA}$ the total volume of a system with mass M, the number of diblock and homopolymer molecules per unit volume can be obtained as:

$$\frac{n_s}{V} = \frac{\varphi_s}{M_s} \times \frac{1}{[v_{PS} + v_{PEO}]\dfrac{\varphi_{PS-PEO}}{M_{PS-PEO}} + v_{PAA}\dfrac{\varphi_{PAA}}{M_{PAA}}} \tag{2}$$

To define the architecture of the molecules, the Gaussian chain contour for the different chain types is discretized into N_α^{scf} repeat units while, for simplicity, the Kuhn segment length, b^{scf}, in the mesoscopic representation is taken to be the same for all species. The requirement of retaining the characteristic size of each chain during the mesoscopic representation leads to:

$$N_\alpha^{scf}(b^{scf})^2 = R_{e(\alpha)}^2 \tag{3}$$

In the following, the end-to-end distance of the diblock, $R_e^2 = R_{e(PS)}^2 + R_{e(PEO)}^2$, sets the characteristic length scale and all lengths will be measured in units of R_e^2. Equation 3 yields:

$$f_\alpha \equiv \frac{N_\alpha^{scf}}{N_{PS}^{scf} + N_{PEO}^{scf}} = \frac{R_{e(\alpha)}^2}{R_{e(PS)}^2 + R_{e(PEO)}^2} \tag{4}$$

where f_α quantifies the ratio of the size of the chains of α species and the diblock. For α = PEO it corresponds to the diblock asymmetry parameter. Because of eq 4, all N_α^{scf} can be expressed as a fraction of the "polymerization degree" of the diblock, $N = N_{PS}^{scf} + N_{PEO}^{scf}$, which constitutes a free parameter of the model. This is the consequence of the fact that the discretization of the Gaussian chain contour (i.e., the definition of the coarse-grained monomer unit) does not have a physical meaning. Equations 2 and 4 summarize the first stage of the model formulation defining the composition of the system and the molecular architecture of our coarse-grained representation.

To proceed further we describe the nonbonded interactions through a functional of the local densities of the different components, formulated as:

$$\begin{aligned}\frac{H}{k_B T} &= \int f[\rho_{PS}(\mathbf{r}), \rho_{PEO}(\mathbf{r}), \rho_{PAA}(\mathbf{r})]\, d\mathbf{r} \\ &= \int \frac{d\mathbf{r}}{R_e^3}\left\{\frac{1}{2}\sum_\alpha\sum_\beta v_{\alpha,\beta}\rho_\alpha(\mathbf{r})\rho_\beta(\mathbf{r}) \right. \\ &\left. + \frac{1}{3}\sum_\alpha\sum_\beta\sum_\gamma w_{\alpha,\beta,\gamma}\rho_\alpha(\mathbf{r})\rho_\beta(\mathbf{r})\rho_\gamma(\mathbf{r})\right\}\end{aligned} \tag{5}$$

where the indices in the summations run over the three different blend components; PS, PEO, and PAA. We explicitly introduced R_e^3 to make the lengths dimensionless. The $\rho_\alpha(\mathbf{r})$ are the dimensionless local density of the chains of species α, defined via the local monomer number densities, $\tilde{\rho}_\alpha(\mathbf{r})$, with the following normalization:

$$\rho_\alpha(\mathbf{r}) = R_e^3 f_\alpha \frac{\tilde{\rho}_\alpha(\mathbf{r})}{N_\alpha^{scf}} = R_e^3 \frac{\tilde{\rho}_\alpha(\mathbf{r})}{N} \tag{6}$$

Contrary to $\tilde{\rho}_\alpha(\mathbf{r})$, the $\rho_\alpha(\mathbf{r})$ do not depend on N_α^{scf} and they describe the spatial distribution of the components independently from the details of the coarse-grained representation. They constitute an *invariant quantity* linking the spatial distribution of the components in our coarse-grained model to the corresponding experimental observations.[34,35] The choice of the excess free energy functional allows to address structure formation in thin films. In this scope, the description of the free polymer surface requires a functional capable of reproducing liquid−vapor coexistence, the minimum condition for which is to have a third-order density dependence. The coefficients, $v_{\alpha,\beta}$ and $w_{\alpha,\beta,\gamma}$, are symmetric with respect to index permutations. They can be related to characteristic thermodynamic properties[38] of the experimental systems, and their values are independent from the choice of N_α^{scf}. Since all lengths are referred to R_e the coefficients $v_{\alpha,\beta}$ and $w_{\alpha,\beta,\gamma}$ as well as the densities, $\rho_\alpha(\mathbf{r})$, are dimensionless.

As a starting point for estimating the coefficients $v_{\alpha,\beta}$ and $w_{\alpha,\beta,\gamma}$, we consider the "diagonal" terms, $\alpha = \beta = \gamma$ related to the thermodynamic properties of the pure components. In this case the mean field free energy of each pure phase can be written as:

$$\frac{FR_e^3}{k_B TV} = \frac{\rho_{o(\alpha)}}{f_\alpha}\ln\left[\frac{\rho_{o(\alpha)}}{f_\alpha}\right] + \frac{1}{2}v_{\alpha,\alpha}\rho_{o(\alpha)}^2 + \frac{1}{3}w_{\alpha,\alpha,\alpha}\rho_{o(\alpha)}^3 \tag{7}$$

The first term of eq 7 represents the translational entropy of the chains and the $1/f_\alpha$ factor accounts for the normalization of ρ_α according to eq 6. The equation of state is then:

$$\frac{PR_e^3}{k_BT} = \frac{\rho_{o(\alpha)}}{f_\alpha} + \frac{v_{\alpha,\alpha}}{2}\rho_{o(\alpha)}^2 + \frac{2w_{\alpha,\alpha,\alpha}}{3}\rho_{o(\alpha)}^3 \quad (8)$$

The requirement $P(\rho_{\mathrm{coex}(\alpha)}) \approx 0$ defines the density of a polymeric liquid coexisting with its vapor under the assumption that, due to the very low density of the vapor, the pressure at coexistence can be considered practically as zero. This coexistence density can be estimated from experimental data as $\rho_{\mathrm{coex}(\alpha)} = R_e^3 f_\alpha \tilde{\rho}^{\mathrm{exp}}_{o(\alpha)}/N^{\mathrm{exp}}_\alpha$ yielding the first equation connecting $v_{\alpha,\alpha}$ and $w_{\alpha,\alpha,\alpha}$ with the thermodynamic properties of the experimental systems. The second thermodynamic relationship required to fully determine the pair $v_{\alpha,\alpha}$ and $w_{\alpha,\alpha,\alpha}$ can be obtained from the compressibility, $\kappa_{T(\alpha)}$, of the polymeric liquid:

$$\frac{R_e^3}{\kappa_{T(\alpha)}k_BT} = -\frac{V}{k_BT}\frac{\partial PR_e^3}{\partial V} = \frac{\rho_{\alpha(o)}}{f_\alpha} + v_{\alpha,\alpha}\rho_{o(\alpha)}^2 + 2w_{\alpha,\alpha,\alpha}\rho_{o(\alpha)}^3 \quad (9)$$

We select the compressibility $\kappa_{T(\alpha)}$ of the components at the coexistence density $\rho_{\mathrm{coex}(\alpha)}$ to be sufficiently high (for specific values used see the next section), so that the density of the phase-separated inhomogeneous system remains approximately uniform. In free-standing films, however, the selection of the coefficients can be further refined to reproduce the experimentally observed preference of the various components to the free surface.

The ten remaining, "non-diagonal" coefficients can be related to the interactions of the PS/PEO/PAA components. The heat of mixing per unit volume $\Delta H_{\alpha,\tilde{\alpha}}/\Delta V$ for each pair $\alpha,\tilde{\alpha}$ can be described via a Van Laar type expression, $\Delta H_{\alpha,\tilde{\alpha}}/\Delta V = D_{\alpha,\tilde{\alpha}}\varphi_\alpha(\mathbf{r})\varphi_{\tilde{\alpha}}(\mathbf{r})$, where $\varphi_\alpha(\mathbf{r})$ and $\varphi_{\tilde{\alpha}}(\mathbf{r})$ are the volume fractions of the α and $\tilde{\alpha}$ components. To this end, we estimate the remaining coefficients considering a ternary PS/PEO/PAA mixture and relating them to the experimentally available $D_{\alpha,\tilde{\alpha}}$'s as

$$\frac{D_{\alpha,\tilde{\alpha}}}{k_BT} = -\frac{1}{2}\frac{\partial^2 f[\varphi_\alpha, 1-\varphi_\alpha-\varphi_{\tilde{\alpha}}, \varphi_{\tilde{\alpha}}]}{\partial^2\varphi_\alpha} \quad (10)$$

where we denote as $\tilde{\tilde{\alpha}}$ the type of the third component. Equation 10 requires the free energy density to be given in terms of volume fractions, which can be trivially obtained from eq 5 taking into account that the volume fractions are related to polymer chain densities as $\varphi_\alpha(\mathbf{r}) = \rho_\alpha(\mathbf{r})/\rho_{\alpha(o)}$. Thus, from eq 10 we obtain:

$$\begin{aligned}\frac{D_{\alpha,\tilde{\alpha}}}{k_BT} = {} & \left[v_{\alpha,\tilde{\alpha}}\rho_{\alpha(o)}\rho_{\tilde{\alpha}(o)} - \frac{v_{\alpha,\alpha}\rho_{\alpha(o)}^2 + v_{\tilde{\alpha},\tilde{\alpha}}\rho_{\tilde{\alpha}(o)}^2}{2}\right] \\ & - [w_{\tilde{\alpha},\tilde{\alpha},\tilde{\alpha}}\rho_{\tilde{\alpha}(o)}^3 + w_{\alpha,\alpha,\tilde{\alpha}}\rho_{\alpha(o)}^2\rho_{\tilde{\alpha}(o)} - 2w_{\alpha,\tilde{\alpha},\tilde{\alpha}}\rho_{\alpha(o)}\rho_{\tilde{\alpha}(o)}^2] \\ & - [w_{\alpha,\alpha,\alpha}\rho_{\alpha(o)}^3 + 3w_{\alpha,\tilde{\alpha},\tilde{\alpha}}\rho_{\alpha(o)}\rho_{\tilde{\alpha}(o)}^2 - w_{\tilde{\alpha},\tilde{\alpha},\tilde{\alpha}}\rho_{\tilde{\alpha}(o)}^3 \\ & - 3w_{\alpha,\alpha,\tilde{\alpha}}\rho_{\alpha(o)}^2\rho_{\tilde{\alpha}(o)}]\varphi_\alpha \\ & - [2w_{\alpha,\tilde{\alpha},\tilde{\alpha}}\rho_{\alpha(o)}\rho_{\tilde{\alpha}(o)}^2 + w_{\alpha,\alpha,\tilde{\tilde{\alpha}}}\rho_{\alpha(o)}^2\rho_{\tilde{\tilde{\alpha}}(o)} + w_{\tilde{\alpha},\tilde{\alpha},\tilde{\tilde{\alpha}}}\rho_{\tilde{\alpha}(o)}^2\rho_{\tilde{\tilde{\alpha}}(o)} \\ & - w_{\alpha,\alpha,\tilde{\alpha}}\rho_{\alpha(o)}^2\rho_{\tilde{\alpha}(o)} - w_{\tilde{\alpha},\tilde{\alpha},\tilde{\alpha}}\rho_{\tilde{\alpha}(o)}^3 - w_{\alpha,\tilde{\alpha},\tilde{\tilde{\alpha}}}\rho_{\alpha(o)}\rho_{\tilde{\alpha}(o)}\rho_{\tilde{\tilde{\alpha}}(o)}]\varphi_{\tilde{\tilde{\alpha}}}\end{aligned} \quad (11)$$

The first term in eq 11 characterizes the dependence of the strength of the interactions on the "second-order" coefficients of the expansion of eq 5 and is proportional to the Flory–Huggins parameter. Analogous expressions have been obtained in other SCF models based on second-order density expansions.[39,40] To this end we require that the strength of the interactions is determined only by the "second-order" coefficients of the density expansion and is independent from composition. Hence the first term in eq 11 is chosen to equal $D_{\alpha,\tilde{\alpha}}/k_BT$ while the remaining terms are set to zero. Taking into account all necessary pair combinations yields a set of equations necessary for the determination of the remaining coefficients and fully defines the model.

Table 1. Values for the "Diagonal" Coefficients $v_{\alpha,\alpha}$ and $w_{\alpha,\alpha,\alpha}$ Calculated for a Mixture of PS-*b*-PEO Diblock with PAA Homopolymers with a Molecular Weight of 10000 g/mol

$v_{PS,PS} = -178.2553665$	$w_{PS,PS,PS} = 4.441\,638$
$v_{PEO,PEO} = -358.2973649$	$w_{PEO,PEO,PEO} = 10.57\,572$
$v_{PAA,PAA} = -312.4444355$	$w_{PAA,PAA,PAA} = 8.616\,953$

Details of the SCFT Calculations. The theoretical and the numerical aspects of the SCFT approach have been extensively presented in the literature.[41−46] In the case when the nonbonded interactions are given by eq 5 the mean fields $W_\alpha(\mathbf{r})$ representing the interactions of a "segment" with its surroundings are obtained as: $W_\alpha(\mathbf{r}) = \delta H/\delta\rho_\alpha(\mathbf{r})$. In the case of the Gaussian chain model the densities, $\rho_\alpha(\mathbf{r})$, can be related to the distribution of the chain conformations in $W_\alpha(\mathbf{r})$ fields, by solving the Edwards diffusion equation. We considered the SCFT equations in one and two dimensions within a real-space scheme.[47] The architecture of the Gaussian chains was defined following eq 4 via the ratios f_{PEO} and f_{PAA} (since $f_{PS} = 1-f_{PEO}$). They require as an input the average squared end-to-end distance for each chain species which are calculated from the experimental systems via an analogue of eq 3: $R_{e(\alpha)}^2 = N_\alpha^{\mathrm{exp}}(b_\alpha^{\mathrm{exp}})^2$, where N_α^{exp} is the polymerization degree of the block or the homopolymer of α species and b_α^{exp} is the size of the corresponding Kuhn segment. For the statistical segment lengths the values $b_{PS}^{\mathrm{exp}} = 0.7$ nm, $b_{PEO}^{\mathrm{exp}} = 0.41$ nm, and $b_{PAA}^{\mathrm{exp}} = 0.55$ nm are used.[48] The polymerization degrees are $N_{PS}^{\mathrm{exp}} = 183$ and $N_{PEO}^{\mathrm{exp}} = 145$, while for the PAA homopolymers we have $N_{PAA}^{\mathrm{exp}} = 74$, $N_{PAA}^{\mathrm{exp}} = 139$, and $N_{PAA}^{\mathrm{exp}} = 279$ (for $M_{PAA} = 5300$, 10000, and 20000 g/mol, respectively). On the basis of this information, to obtain the proper molecular asymmetry, in the SCFT calculations the chain contours were discretized using the following number of segments: $N_{PS-PEO}^{\mathrm{scf}} = 1540$ (with $N_{PS}^{\mathrm{scf}} = 1200$, $N_{PEO}^{\mathrm{scf}} = 340$), for the diblock and $N_{PAA}^{\mathrm{scf}} = 300$, 568 and 1140 for the PAA homopolymer, depending on the molecular weight. The spatial discretization in 2D was $\Delta \approx 0.037\ R_{PS-PEO}$, while in 1D we typically used $\Delta \approx 0.01\ R_{PS-PEO}$. The free energies of the lamella (LAM) and the hexagonally packed cylinder (CYL) morphologies were determined in 1D and 2D calculations after optimizing the dimensions of the unit cell. To establish the convergence of the iterative procedure, the relative accuracy of the scheme, Γ_α, was monitored following ref 49. Typically, a convergence on the order of $\Gamma_\alpha \sim 10^{-10}$ was obtained.

The pure phase densities needed as an input for eqs 8 and 9 are calculated from $\rho_{o(\alpha)} = R_{PS-PEO}^3 f_\alpha \tilde{\rho}^{\mathrm{exp}}_{o(\alpha)}/N^{\mathrm{exp}}_\alpha$. For simplicity all the three species are assumed to have the same material density 1 g/cm^3. We use for compressibility the values $\kappa_{T(PEO)} = \kappa_{T(PAA)} \approx 0.86\times10^{-5}R_e^3/k_BT$ and $\kappa_{T(PS)} \approx 0.12\times10^{-4}R_e^3/k_BT$. The "diagonal" coefficients obtained for the PS and the PEO components are given in the Table 1, where we also present the set of the "diagonal" coefficients $v_{PAA,PAA}$ and $w_{PAA,PAA,PAA}$ calculated for the representative case of the PAA homopolymers with MW 10000 g/mol.

For calculating the remaining "mixed" coefficients, experimental estimates of the $D_{\alpha,\tilde{\alpha}}$ parameters are available. For example in ref [50] the values $D_{PS,PEO} = 7.53$ J/cm^3, $D_{PS,PAA} = 153.13$ J/cm^3, and $D_{PEO,PAA} = -64.852$ J/cm^3 are reported.

Table 2. Values for the "Off-Diagonal" Coefficients $v_{\alpha,\beta}$ and $w_{\alpha,\beta,\gamma}$ Calculated for a Mixture of PS-*b*-PEO Diblock with PAA Homopolymers with a Molecular Weight of 10000 g/mol

$v_{PS,PEO} = -255.01294710$	$w_{PS,PS,PEO} = 6.019\,095$
	$w_{PS,PEO,PEO} = 8.028\,496$
$v_{PS,PAA} = -237.49$	$w_{PS,PS,PAA} = 5.621\,811$
	$w_{PS,PAA,PAA} = 7.003\,698$
$v_{PEO,PAA} = -335.796$	$w_{PEO,PEO,PAA} = 9.877\,750$
	$w_{PEO,PAA,PAA} = 9.225\,839$
$w_{PS,PEO,PAA} = 14.99\,722$	

The high immiscibility of the PS/PAA pair is manifested by the large positive value of $D_{PS,PAA}$. The negative $D_{PEO,PAA}$ value indicates a strong affinity between the two components due to the formation of hydrogen bonds.[50] Unfortunately, exploratory SCFT calculations performed using the coefficients obtained from the experimentally available $D_{\alpha,\tilde{\alpha}}$ demonstrated that the interfaces are too narrow to allow a sufficiently accurate 2D description within the spatial discretization of the numerical scheme. The magnitude of Δ used in the 2D calculations restricted our SCFT calculations to mixtures with PAA concentrations up to 20% and required the reduction of the degree of segregation between the different components. Choosing $D_{PS,PEO} = 6.50$ J/cm^3, $D_{PS,PAA} = 9$ J/cm^3, and $D_{PEO,PAA} = -4$ J/cm^3 allowed us to span the concentration range, $0 \leq \varphi_{PAA} \leq 0.2$, for all the PAA molecular weights that have been considered, and to avoid interface registration effects (i.e., faceted cylinders). At the same time this choice of $D_{\alpha,\tilde{\alpha}}$ mimics the relative strength of the interactions in the experimental system, in the spirit of similar theoretical approaches that have been used for systems with specific interactions.[16,51] Using these interactions as an input and following the approach outlined after eq 11 the calculation of the remaining coefficients is straightforward. The "non-diagonal" coefficients calculated for the case of a PS-*b*-PEO diblock mixture with PAA homopolymers of MW 10000 g/mol, are shown in Table 2. For all calculations the temperature was taken to be $T = 423$ K. The interaction coefficients used for the blends with 5300 and 20000 g/mol PAA are provided in the Tables S1−S4 in the Supporting Information.

Results and Discussion

The PS_{19}-*b*-$PEO_{6.4}$ copolymer, with a PEO volume fraction of 0.23, was the first studied. Two PAA were chosen: $PAA_{5.3}$ (DP = 74) which is smaller than the PEO block (DP = 145), and PAA_{20} which is larger (DP = 277). THF solutions of the copolymer with different amounts (expressed as weight fractions with respect to the copolymer) of $PAA_{5.3}$ and PAA_{20} were prepared and were deposited by spin-coating on silicon substrates. The resulting thin films were imaged by SFM, and representative examples are shown in Figure 1. For both PAA, cylindrical microdomains oriented perpendicularly to the film surface are clearly seen for the lower PAA fractions. For higher fractions, a transition toward a lamellar morphology is observed. The first interesting point to be noted is the exclusive formation of perpendicular cylinders at low and intermediate PAA fractions. The pristine PS_{19}-*b*-$PEO_{6.4}$ copolymer self-assembles, under the same preparation conditions, into a mixed orientation of parallel and perpendicular cylinders (see Figure 2). The self-assembly of PS-*b*-PEO copolymers is known to be very sensitive to the preparation conditions (solvent used, ambient humidity, ...),[52,53] but when even small amounts of PAA are blended with PS-*b*-PEO, perpendicular cylinders are always formed in a rather large range of experimental conditions. Indeed, films of PS-*b*-PEO/PAA blends were prepared on hydrophilic (piranha cleaned) and hydrophobic (treated with hexamethyldisilazane, HMDS) silicon substrates, and the film thickness was varied from 50 to 250 nm, yielding exclusively perpendicular cylinders in all cases. To ensure that the cylindrical domains spanned across the entire thickness of the films, a 150 nm film was prepared on a silicon substrate covered with a 400 nm thick silicon oxide layer. The film was floated onto the surface of a dilute hydrofluoric acid solution (5 wt %) and transferred to a water bath. Using a clean silicon slide the copolymer film was then transferred upside down onto the slide such that the bottom of the original film was now on the top. The SFM image of this sample (Figure 3) shows that the cylindrical microdomains are present at the bottom of the film, suggesting that the microdomain orientation propagates through the entire film. This increased tendency to form perpendicular cylinders observed in our experiments has been previously reported for other blends self-assembled in thin films, and has been tentatively attributed to two possible causes. The first one constitutes a

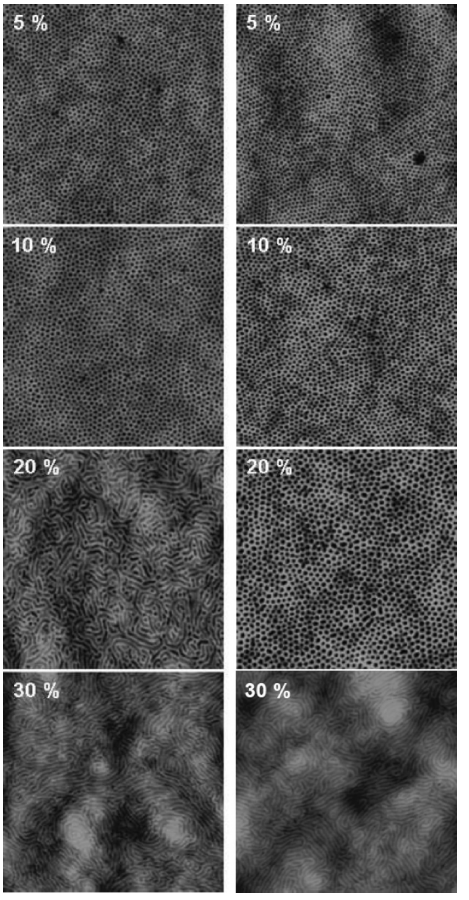

Figure 1. SFM height images (2×2 μm^2) recorded on thin films of mixtures of PS_{19}-*b*-$PEO_{6.4}$ with different weight fractions of $PAA_{5.3}$ (left column) and PAA_{20} (right column).

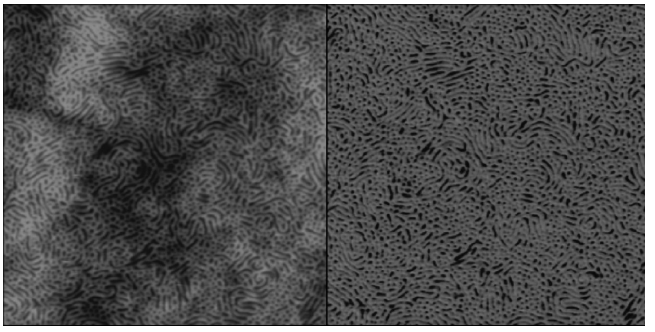

Figure 2. SFM images (left, height; right, phase, 2×2 μm^2) recorded on a thin film of the pristine PS_{19}-*b*-$PEO_{6.4}$ copolymer.

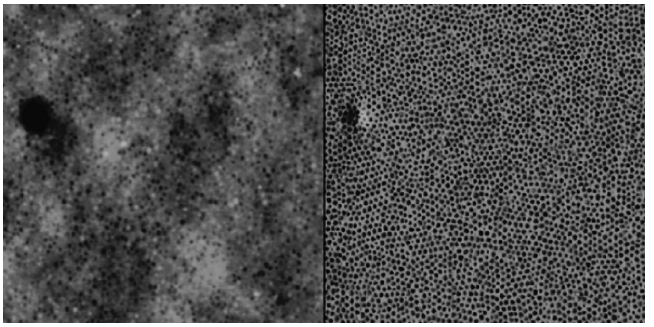

Figure 3. SFM images (left, height; right, phase, $2 \times 2\ \mu m^2$) recorded on the bottom surface of a thin film of a mixture of PS_{19}-*b*-$PEO_{6.4}$ with 20% of PAA_{20}.

phenomenological argument[24] motivated by experimental evidence that the domain-matrix excess free energy is considerably increased during the reorientation of the cylinders from parallel to perpendicular. Hence a thermodynamic compensating force should exist to favor this rearrangement. This favorable contribution could be enthalpic, originating from an increase of incompatibility, compared to the pristine copolymer, between the matrix and the dispersed phase and/or from an intermolecular affinity between the homopolymer and its corresponding block component.[24] The second one is the confinement of the homopolymer to the center of the cylinders inducing a stretching of the chains along the axis of the latter.[23] In the present case, both factors could play a role in explaining the perpendicular orientation of the cylinders. It has indeed been recently reported that the blending of PEO-based copolymers with some additives (inorganic salts or PAA) could induce an increase of incompatibility toward the other block,[51,54] and moreover there is a strong affinity between PEO and PAA. In addition, the Flory−Huggins parameter χ between PS and PAA is around 0.3[55] and is thus much higher than the χ parameter between PS and PEO, which is only around 0.03.[56] Therefore, it is expected that the PAA will be localized in the center of the PEO cylinders in order to minimize the contacts with the PS matrix (see below).

As already mentioned, a transition to a lamellar morphology occurs for both PAA as the homopolymer fraction increases. This behavior is different from previous literature results on thin films of blends of the same PS-*b*-PEO copolymer with PEO or PMMA homopolymers.[22] In this case, no transition of morphology was observed, but instead a macrophase separation was quickly reached as the PEO or PMMA fraction increased, especially for higher molecular weight homopolymers. In our case, the enhanced compatibility, enabling the observation of a morphological transition, is due to the highly favorable enthalpic interactions between the PEO block and the PAA homopolymer, which can interact via hydrogen bonds. However, a closer look at Figure 1 reveals that this transition takes place at a smaller fraction for $PAA_{5.3}$ than for PAA_{20}. In the case of $PAA_{5.3}$, the transition already occurs at 20% of PAA, while a fraction of 30% has to be reached for PAA_{20}.

The experimental observations regarding the dependence of the morphology on the PAA concentration and molecular weight can be directly compared with the SCFT predictions. Figure 4 presents the free energy difference (per unit volume), $(F_{cyl} - F_{lam})/V$, of the CYL and the LAM morphologies as a function of the PAA concentration, obtained via SCFT, for three different molecular weights of PAA: 5300 (triangles), 10000 (squares), and 20000 (circles) g/mol. For this selection of PAA homopolymers, the SCFT predicts a weak influence of the homopolymer molecular weight on the functional dependence of $(F_{cyl} - F_{lam})/V$ on the amount of PAA homopolymer. Figure 4 indicates that the LAM morphology becomes less favorable compared to the

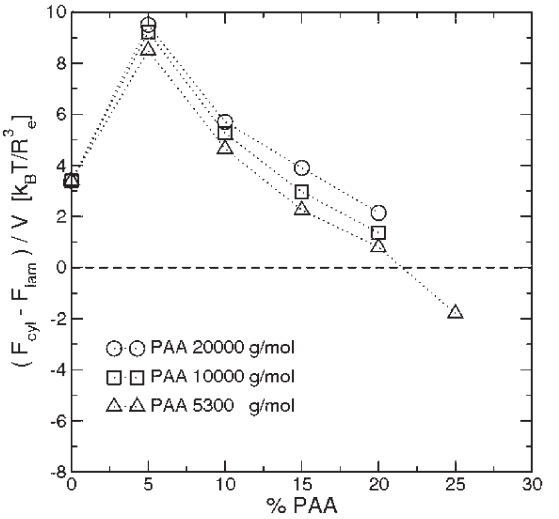

Figure 4. SCFT prediction for the difference of the free energies between the cylindrical and the lamellar phases as a function of the PAA content in the blend, calculated for three different molecular weights of PAA homopolymer: 5300 g/mol (triangles), 10000 g/mol (squares), and 20000 g/mol (circles).

CYL, as the molecular weight of the PAA increases. For the 5300 g/mol PAA, the SCFT places the CYL to LAM transition between 20 and 25% of PAA, while for the two longer homopolymers the transition point extrapolates to somewhat higher PAA concentrations. The SCFT calculations follow qualitatively the experimental observations with respect to the value of the PAA concentration, at which the morphology changes from CYL to LAM and its dependence on the PAA homopolymer molecular weight. A quantitative comparison is not possible because of the reduced segregation of the PS/PEO/PAA components (compared to the experiments), of the fact that the SCFT calculations refer to bulk blends, and of the simplified description of the hydrogen bonding, which is accounted in the SCFT model simply through a constant, negative value of the PEO/PAA χ parameter.

As mentioned above, while discussing the increased tendency of the blends to form perpendicular cylinders, the PAA homopolymer seems to be segregated to the center of the cylindrical domains. Experimental evidence of this can be obtained by monitoring the evolution of the lattice spacing with the amount of PAA added. In particular, the lattice spacing, *D*, was measured on the SFM images by using the 2D power spectral density routine of the Nanoscope program. For the addition of the PAA_{20} homopolymer, *D* increases from about 37 nm to about 47 nm when going from the pristine PS-*b*-PEO copolymer to the blend with 20% PAA, the highest concentration still showing perpendicular cylinders. For the blends with $PAA_{5.3}$, *D* seems to increase in a similar manner as for the blends with PAA_{20}, but the measurable range is more limited since for $PAA_{5.3}$ the highest concentration yielding perpendicular cylinders is only 10% of PAA. The substantial increase of the lattice spacing *D* with the amount of added PAA is a strong indication that the PAA is not homogeneously distributed in the PEO cylinders but instead is segregated in the center of the cylinders. It has been indeed previously reported for other blends that a homogeneous distribution of the homopolymer in the microdomains does not lead to a significant swelling of the latter, and that a segregation of the homopolymer inside the microdomains was required to observe such swelling, and thus an important increase of the lattice spacing.[4,9]

The PAA enrichment in the core of the cylindrical domains suggested by the experimental data is in full agreement with the

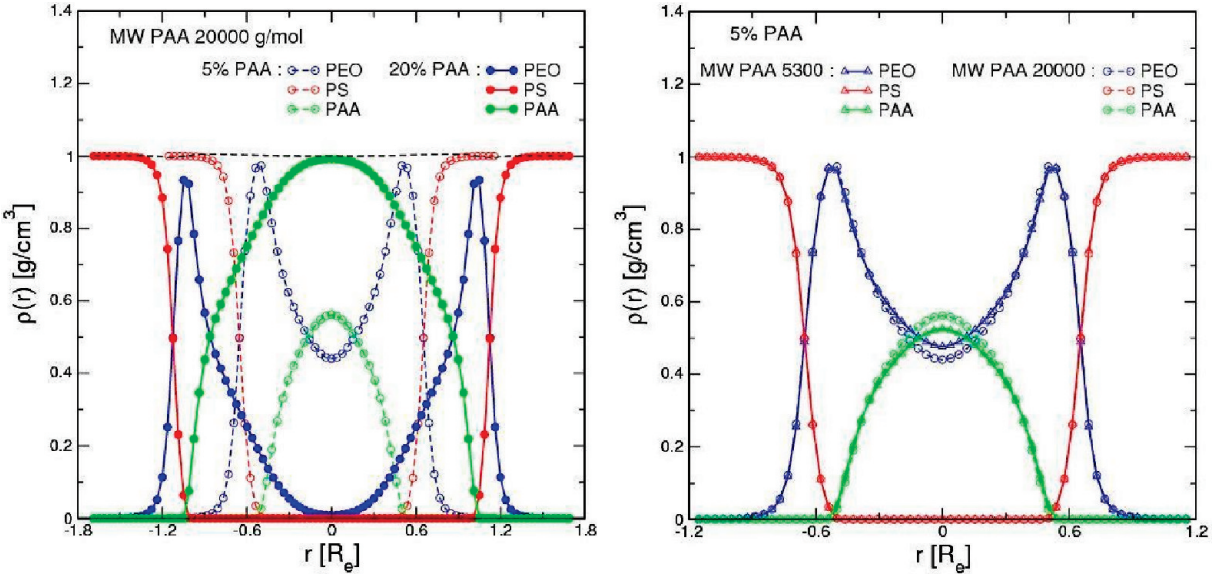

Figure 5. Shown on the left are the density profiles across a cylindrical domain, obtained via the SCFT calculations, for the PS (red symbols), PEO (blue symbols), and PAA (green symbols) components. The graph shows results for blends containing 5% (open symbols) and 20% (solid symbols) of PAA with a molecular weight 20000 g/mol. The dashed black line marks the total density profile for the blend with 20% of PAA. The right panel shows a comparison between the density profiles of the three components obtained for two different PAA molecular weights 5300 g/mol (triangles) and 20000 g/mol (circles) for two blends with 5% of PAA content.

SCFT results. As a demonstration, we show in the left panel of Figure 5 the density profiles of the PS (red symbols), PEO (blue symbols), and PAA (green symbols) components across a cylindrical domain, for blends containing 5% (open symbols) and 20% (solid symbols) of PAA. The molecular weight of the PAA in the blends considered in the left panel is 20000 g/cm^3. From the profiles it can be seen that the PAA homopolymer always tends to be segregated toward the center of the cylindrical domain. The PEO block of the PS_{19}-*b*-$PEO_{6.4}$ diblock "coats" the PAA-rich core of the cylinder, even in the case of blends with a relatively high PAA content, so that the number of contacts between the PAA homopolymer and the PS matrix surrounding the cylinders is minimized. As was mentioned before, although the absolute strength of the interactions is lower in the SCFT calculations, their relationship is similar to the experimental systems, i.e., as in the experimental systems, in the SCFT model the PS/PAA pair is much more immiscible comparing to the PS/PEO pair, while at the same time there is a strong affinity between PEO and PAA. Hence it is believed that the coaxial layering of the PEO and PAA components within the cylindrical domains, observed in SCFT calculations, corresponds to the situation encountered in the experiments and has the same origin, i.e., the relative strength of interactions in the system. To demonstrate that the values of the compressibility coefficients employed during the SCFT calculations are sufficient for approximating the limit of an almost incompressible liquid, the total density profile across the cylindrical domain is also plotted (dashed black line) for the blend with 20% of PAA. It can be seen that, even for this strongly segregated system, the total density profile varies very little across the domain interfaces.

The calculations predict that, for the considered range of molecular weights, the dependence of the domain structure on the molecular weight of the PAA homopolymer is very weak. To demonstrate this, we show in the right panel of Figure 5 a comparison of the density profiles across a cylindrical domain obtained for mixtures containing 5% of PAA with molecular weight 5300 g/mol (triangles) and 20000 g/mol (circles). In this case, the molecular weight of the PAA mostly affects the internal structure of the cylinder: The PAA segregation to the center is somewhat higher in the case of the longest homopolymer. This

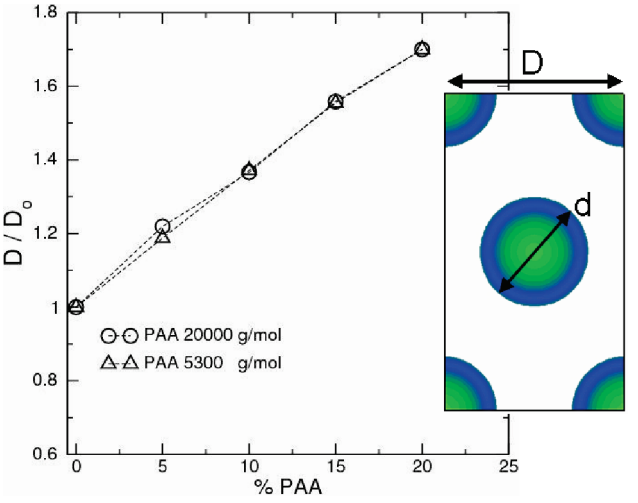

Figure 6. The main panel shows the SCFT predictions for the dependence of the lattice spacing of the cylindrical morphology on the PAA homopolymer content in the blend for PAA of two different molecular weight: 5300 g/mol (triangles) and 20000 g/mol (circles). The inset shows a unit cell of the cylindrical morphology obtained with SCFT for a blend containing 10% of PAA with molecular weight 5300 g/mol. For clarity only the PEO (blue) and PAA (green) phases are shown while the characteristic dimensions of the structure *D* and *d* are also marked on the plot.

can be rationalized considering that the longer PAA homopolymers tend to penetrate less the "brush" region of the PEO blocks of the diblock that are anchored at the interface with the PS matrix. However, this effect is small, hence it is expected that the domain properties will be mostly driven by the "bare" amount of PAA in the mixture regardless of the PAA molecular weight. As a consequence, the SCFT calculations predict that the dependence of the cylinder size, *d*, and spacing, *D*, on the PAA content will be very similar for the three different PAA molecular weights that have been considered. The definition of both characteristic structure dimensions is clarified in the inset of Figure 6, showing a representative morphology obtained with SCFT for a blend

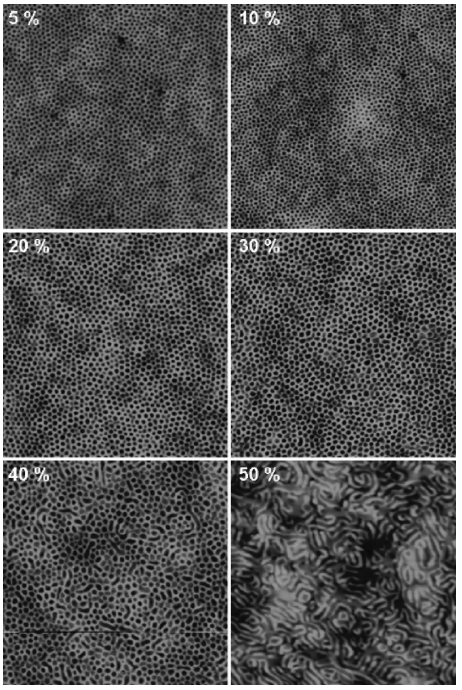

Figure 7. SFM height images (2×2 μm^2) recorded on thin films of mixtures of PS_{37}-*b*-$PEO_{6.5}$ with different weight fractions of $PAA_{5.3}$.

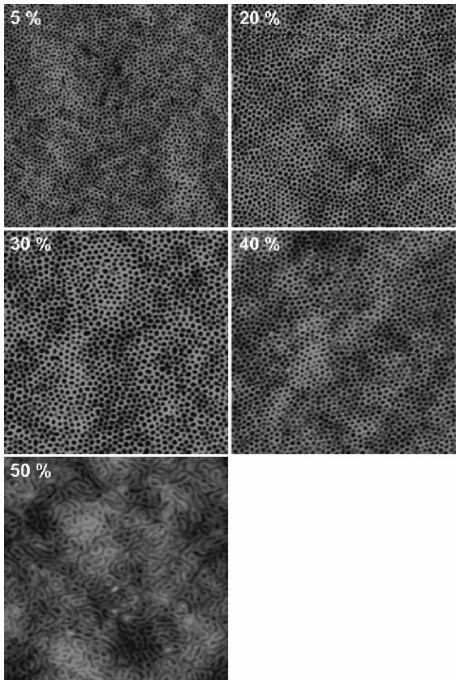

Figure 8. SFM height images (2×2 μm^2) recorded on thin films of mixtures of PS_{37}-*b*-$PEO_{6.5}$ with different weight fractions of PAA_{20}.

containing 10% of PAA with molecular weight 5300 g/mol. The main panel of Figure 6, presents the SCFT predictions for the evolution of the cylinder spacing, D, as a function of the PAA amount for the two limiting molecular weights of PAA: 5300 g/mol (triangles) and 20000 g/mol (circles). The spacing is normalized to the distance between the cylinders in the pristine PS_{19}-*b*-$PEO_{6.4}$ copolymer, D_o. In analogy to the experimental observations the SCFT model predicts that the increase of the PAA content leads to a notable swelling of the cylinders: for instance, the hexagonal lattice spacing in the blend containing 20% PAA is 1.7 times larger compared to the pristine diblock system. As discussed above, the dependence of D on the PAA concentration is very similar for both molecular weights, i.e., within the numerical accuracy of our approach the corresponding curves almost overlap.

The SCFT prediction that the CYL morphologies in blends with homopolymers of different PAA molecular weights but the same "bare" amount of PAA should have similar features, were confirmed by additional experiments. Unfortunately, the experimental data reported above for blends of the PS_{19}-*b*-$PEO_{6.4}$ copolymer with PAA did not allow us a thorough investigation of this issue since in the blends with the shortest $PAA_{5.3}$ homopolymer the transition of morphology occurred at a rather low PAA content (between 10% and 20%). Therefore, we considered systems where a more asymmetric copolymer, PS_{37}-*b*-$PEO_{6.5}$, has been used as a starting point for the blends. This copolymer has a much larger PS block, while keeping the same PEO block length, compared to the previous copolymer, resulting in a PEO volume fraction of only 0.13. This low fraction of PEO enabled us to add more PAA before reaching the lamellar regime, and thus to have a better observation of the evolution of the characteristics of the cylindrical phase with increasing content of PAA. As for the other copolymer, a film of the pristine PS_{37}-*b*-$PEO_{6.5}$ copolymer shows a mixed orientation of the PEO cylinders (see figure S1 in the Supporting Information). Different amounts of $PAA_{5.3}$ and PAA_{20} were then blended with the PS_{37}-*b*-$PEO_{6.5}$ and thin films were prepared. Their representative SFM images are shown in Figures 7 and 8. The evolution of the features of the thin films with increasing amount of PAA is very similar to the one observed previously for the PS_{19}-*b*-$PEO_{6.4}$ copolymer. Indeed, the addition of PAA induces an orientation of the cylindrical microdomains perpendicularly to the film surface, and a transition of morphology is observed for high PAA fractions. As expected this transition occurs at higher PAA content (around 40−50%) for the PS_{37}-*b*-$PEO_{6.5}$ copolymer than for the PS_{19}-*b*-$PEO_{6.4}$ copolymer (around 20−30%) since the starting PEO fraction is lower, and thus more PAA has to be blended to reach a composition giving rise to a morphological transition. Nevertheless, for a PAA of a given molecular weight, the global composition at which this transition occurs is the same for both copolymers. For $PAA_{5.3}$ the volume fraction of (PEO+PAA) where the transition is observed is equal to 0.33 for both copolymers, and is equal to 0.37 for PAA_{20}. This also confirms that the transition occurs at lower PAA content for the $PAA_{5.3}$ than for the PAA_{20}.

The larger amount of PAA that could be added in the new system, while preserving the CYL morphology, allowed us to explore systematically the evolution of the lattice spacing, D, as a function of the blend composition for the different molecular weights of PAA. The dependence of D on the amount of PAA is shown in Figure 9 for both PAA homopolymers, where a clear and regular increase of the lattice spacing with the amount of PAA added is observed. At the same time the graph demonstrates that both kinds of PAA (i.e., the 5300 g/mol and the 20000 g/mol) give rise to a similar evolution, in full agreement with the SCFT predictions (see above and Figure 6).

The size of the cylindrical domains, d, constitutes an additional structural property of interest. To this end, in Figure 10, we report the SCFT predictions concerning the dependence of the diameter of the domains on the amount of the added PAA. The diameters have been normalized to the size of the cylinders, d_o, measured in the pristine PS_{19}-*b*-$PEO_{6.4}$ copolymer. It can be seen that the evolution of d/d_o as a function of the amount of PAA added, is very similar to the evolution of the lattice spacing, D/D_o, shown in Figure 6. The comparable dependence of d and D on the PAA amount can be rationalized by taking into account that in the case of the systems considered in this work, due to the strong segregation between the PS matrix and the PEO and PAA

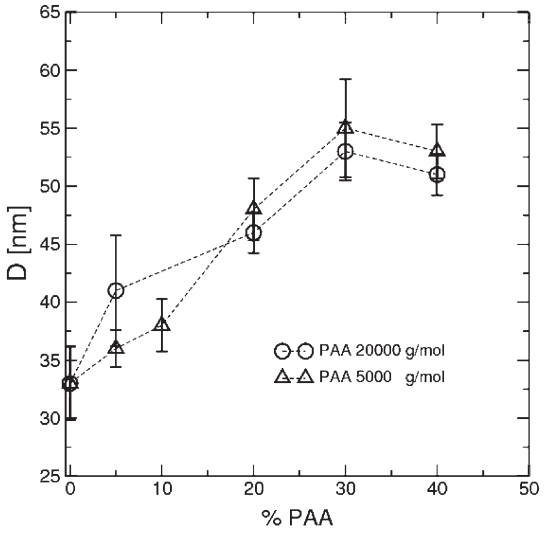

Figure 9. Evolution of the lattice spacing, measured on SFM images, as a function of the weight fraction of PAA added in PS_{37}-*b*-$PEO_{6.5}$.

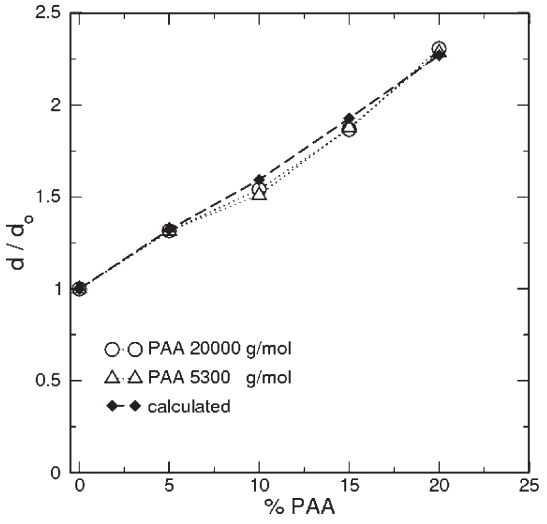

Figure 10. SCFT predictions for the dependence of the normalized diameter of the cylinders on the PAA homopolymer content in the blend for two PAA of different molecular weight: 5300 g/mol (triangles) and 20000 g/mol (circles). The solid rhombus symbols with the dashed line denote the estimation derived from a simple volumetric argument (see main text).

components, *d* and *D* can be related through a simple, volumetric argument. We consider the case of a unit cell containing two cylinders (see inset of Figure 6) where the total area of the cell is $S = \sqrt{3}D^2$ while the area corresponding to the PAA and PEO components is $S_{PAA} = \sqrt{3}D^2\varphi_A$ and $S_{PEO} = \sqrt{3}D^2(1-\varphi_A)f_{PEO}$ respectively. Then the cylinder diameter, *d*, is connected to the lattice spacing *D* via: $\pi d^2/4 = 1/2\,[(1-\varphi_A)f_{PEO} + \varphi_A]\sqrt{3}D^2$. The result of this simple volumetric estimation of *d*, obtained for the 20000 g/mol PAA blends using the lattice spacings reported in Figure 6, is marked in Figure 10 with solid rhombus symbols/dashed line and follows closely the results of SCFT.

The amount of relative swelling, d/d_o, of the cylinders with respect to the different amounts of PAA added was estimated experimentally for the case of the blends based on the PS_{37}-*b*-$PEO_{6.5}$ copolymer. Representative graphs are reported in Figure 11, where the diameters *d* and d_o were obtained after analyzing the SFM images. Figure 11 evidence that both molecular weights of PAA give rise to a similar swelling degree of the cylinders, in full agreement with the SCFT results. The observed degree of swelling is also in good agreement with the one estimated from the simple volumetric arguments (solid rhombus symbols/dashed line). The latter point serves as an additional confirmation of the fact that the quantity of PAA homopolymer potentially present in the PS matrix is negligible, and that the spots on the free surface of the film correspond indeed to the top of vertical cylinders with straight walls. In particular, it is possible to exclude cylindrical barrel-like structures, reported for instance in refs 57 and 58, which could appear in the case of a weak preference of the PS or the PEO/PAA components for the polymer/air interface (see inset of Figure 11).

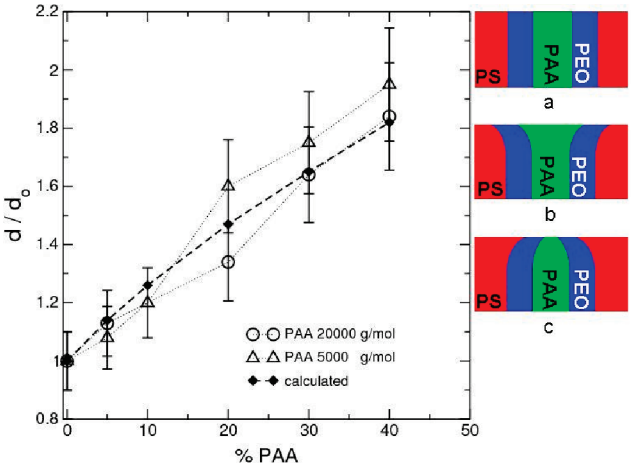

Figure 11. The graph in the main panel shows the evolution of the normalized cylinder diameter, measured on SFM images, as a function of the weight fraction of PAA added in PS_{37}-*b*-$PEO_{6.5}$. The solid rhombus symbols with the dashed line correspond to the estimation obtained from a volumetric argument. The cartoon in the inset illustrates the possible shapes of the cylindrical domains near the free surface of the polymer film for the cases when the polymer/air interface is (a) neutral to the three components, (b) slightly PEO/PAA preferential, and (c) slightly PS preferential. The measured size of the domains and the one estimated from the simple volumetric argument will match only in the first case.

Previous studies have shown that the evolution of the characteristic length scale of the microdomains (lattice spacing, diameter) with homopolymer content will depend on the molecular weight of the added homopolymer only until a certain critical value, above which this parameter does not influence the evolution anymore.[4,9] In our case, the fact that both the experiments and the SCFT calculations show that the characteristics of the microdomains are practically independent from the PAA molecular weight, demonstrates that even the shortest homopolymer that has been considered, $PAA_{5.3}$, is already above this critical value.

Conclusions

We have shown that the addition of PAA can be used to tune the self-assembly of PS-*b*-PEO block copolymers in thin films. PAA interacts specifically with PEO by hydrogen bonding and is thus located exclusively within the PEO microdomains. The presence of PAA induces an orientation of the cylindrical microdomains perpendicularly to the film surface, even for small weight fractions, and in a broad range of experimental conditions. Moreover, the lattice spacing increases regularly with the amount of PAA added up to a point where a transition toward a lamellar morphology is observed. This transition occurs at lower PAA content for PAA of small molecular weight. This behavior is different from the one of other AB + C blends, where no strong specific interactions are present, which exhibit a macrophase separation upon increasing the homopolymer fraction. All those

observations indicate that the PAA homopolymer is not homogeneously mixed with PEO but is rather localized in the center of the PEO microdomains, in a cylinder within a cylinder fashion.

The experimental observations were compared with the predictions of SCFT calculations based on a model defining the nonbonded interactions through a functional capable of reproducing liquid−vapor coexistence due to a third-order dependence on the local densities of the different components. Here we employed two-dimensional SCFT calculations to address the domain properties in the "bulk" of PS-*b*-PEO/PAA blends. Nevertheless, the model can be straightforwardly employed for a three-dimensional study of structure formation in polymeric films. When applied to these systems, the potential advantages of the model include the ability to describe the topography of the free surface (e.g., island/hole formation). This is not the case for the Helfands' quadratic density functional which is most frequently used in the literature for SCFT modeling of compressible polymeric liquids. An additional attractive feature of the model is that its parameters can be straightforwardly related to several characteristic thermodynamic quantities such as the density and the compressibility of the pure components, the heat of mixing, and the ratio of the surface free energies of the different components.

The SCFT calculations reproduce qualitatively the experimental dependence of the morphology on the amount of PAA added as a function of the molecular weight of the homopolymer. Namely they also show that in the case of longer homopolymers the CYL to LAM transition occurs at higher PAA concentrations. The profiles of the spatial distribution of the components within the cylindrical domains obtained in the SCFT calculations confirm the suggestion that the PAA homopolymers are localized in the center of the cylindrical domains. In full agreement with the trends observed experimentally, the calculations suggest that for the different molecular weights of PAA, the properties of the microdomains (the spacing and the dimensions of the cylinders) are affected by the amount of PAA added in a very similar way.

The PS-*b*-PEO/PAA blends are a promising system to easily tune the thin film characteristics (lattice spacing, cylinder diameter, morphology) in a very broad range. It is thus an interesting candidate for diverse applications in nanotechnology—even more so since the removal of the PAA homopolymer can be envisaged by simple rinsing with water to create nanoporous thin films.[59]

Acknowledgment. N.L. thanks the FRIA for financial support. C.-A.F. is Research Associate of the FRS-FNRS. The authors are grateful to the STIPOMAT Program from the European Science Foundation. J.-F.G. and C.-A.F. thank BELSPO for financial support in the frame of the network IAP 6/27. K.Ch.D and M.M. acknowledge funding by the VW foundation and the DFG under grant Mu1674/9.

Supporting Information Available: Tables of values for the different "diagonal" and "off-diagonal" coefficients calculated for the mixtures of PS-*b*-PEO diblock with different PAA homopolymers, text discussing the SCF models and figures showing additional SFM and SEM images. This material is available free of charge via the Internet at http://pubs.acs.org.

References and Notes

(1) Ruzette, A. L.; Leibler, L. *Nat. Mater.* **2005**, *4*, 19.
(2) Abetz, V. P.; Simon, F. W. *Adv. Polym. Sci.* **2005**, *189*, 125.
(3) (a) Hamley, I. W. *Angew. Chem., Int. Ed.* **2003**, *42*, 1692. (b) Smart, T.; Lomas, H.; Massignani, M.; Flores-Merino, M. V.; Ruiz Perez, L.; Battaglia, G. *Nanotoday* **2008**, *3*, 38.
(4) Hashimoto, T.; Tanaka, H.; Hasegawa, H. *Macromolecules* **1990**, *23*, 4378.
(5) Hashimoto, T.; Tanaka, H.; Hasegawa, H. *Macromolecules* **1991**, *24*, 240.
(6) Mayes, A. M.; Russell, T. P.; Satija, S. K.; Majkrzak, C. F. *Macromolecules* **1992**, *25*, 6523.
(7) Löwenhaupt, B.; Steurer, A.; Hellmann, G. P.; Gallot, Y. *Macromolecules* **1994**, *27*, 908.
(8) Torikai, N.; Takabayashi, N.; Noda, I.; Koizumi, S.; Morii, Y.; Matsushita, Y. *Macromolecules* **1997**, *30*, 5698.
(9) Jeong, U.; Ryu, D.; Kho, D.; Lee, D.; Kim, J.; Russell, T. P. *Macromolecules* **2003**, *36*, 3626.
(10) Banaszak, M.; Whitmore, M. D. *Macromolecules* **1992**, *25*, 2757.
(11) Matsen, M. *Macromolecules* **1995**, *28*, 5765.
(12) Janert, P. K.; Schick, M. *Macromolecules* **1998**, *31*, 1109.
(13) Matsen, M. *Macromolecules* **2003**, *36*, 9647.
(14) Hashimoto, T.; Kimishima, K.; Hasegawa, H. *Macromolecules* **1991**, *24*, 5704.
(15) Denesyuk, N. A.; Gompper, G. *Macromolecules* **2006**, *39*, 5497.
(16) Klymko, T.; Subbotin, A.; Ten Brinke, G. *Macromolecules* **2007**, *40*, 2863.
(17) Dobrosielska, K.; Wakao, S.; Takano, A.; Matsushita, Y. *Macromolecules* **2008**, *41*, 7695.
(18) Chen, W. C.; W. Kuo, S.; Jeng, U. S.; Chang, F. C. *Macromolecules* **2008**, *41*, 1401.
(19) Lee, J. H.; Balsara, N. P.; Chakraborty, A. K.; Krishnamoorti, R.; Hammouda, B. *Macromolecules* **2002**, *35*, 7748.
(20) For reviews on polymer blends involving hydrogen bond, see, for example: (a) He, Y.; Zhu, Y.; Inoue, B. *Prog. Polym. Sci.* **2004**, *29*, 1021. (b) Kuo, S. W. *J. Polym. Res.* **2008**, *15*, 459.
(21) van Zoelen, W.; ten Brinke, G. *Soft Matter* **2009**, *5*, 1568.
(22) Kim, S.; Misner, M.; Russell, T. *Adv. Mater.* **2004**, *16*, 2119.
(23) Jeong, U.; Ryu, D. Y.; Kho, D. H.; Kim, J. K.; Goldbach, J. T.; Kim, D. H.; Russell, T. P. *Adv. Mater.* **2004**, *16*, 533.
(24) (a) Ahn, D. U.; Sancaktar, E. *Soft Matter* **2008**, *4*, 1454. (b) Ahn, D. U.; Sancaktar, E. *Adv. Funct. Mater.* **2006**, *16*, 1950.
(25) Kitano, H.; Akasaka, S.; Inoue, T.; Chen, F.; Takenaka, M.; Hasegawa, H.; Yoshida, H.; Nagano, H. *Langmuir* **2007**, *23*, 6404.
(26) Jeong, U.; Kim, H. C.; Rodrigez, R. L.; Tsai, I. Y.; Stafford, C. M.; Kim, J. K.; Hawker, C. J.; Russell, T. P. *Adv. Mater.* **2002**, *14*, 274.
(27) Mykhaylyk, T. A.; Mykhaylyk, O. O.; Collins, S.; Hamley, I. W. *Macromolecules* **2004**, *37*, 3369.
(28) Li, X.; Zhao, S.; Kim, D. H.; Knoll, W. *Langmuir* **2007**, *23*, 6883.
(29) Tang, C.; Lennon, E. M.; Fredrickson, G. H.; Kramer, E. J.; Hawker, C. J. *Science* **2008**, *322*, 429.
(30) (a) Bang, J.; Jeong, U.; Ryu, D. Y.; Russell, T. P.; Hawker, C. J. *Adv. Mater.* **2009**, *21*, 4787. (b) Hamley, I. W. *Prog. Polym. Sci.* **2009**, *34*, 1161.
(31) Hillmyer, M. A. *Adv. Polym. Sci.* **2005**, *190*, 137.
(32) Stoykovich, M. P.; Müller, M.; Kim, S. O.; Solak, H. H.; Edwards, E. W.; de Pablo, J. J.; Nealey, P. F. *Science* **2005**, *308*, 1442.
(33) Stoykovich, M. P.; Kang, H.; Daoulas, K. Ch.; Liu, G.; Liu, C. C.; de Pablo, J. J.; Müller, M.; Nealey, P. F. *ACS Nano* **2007**, *1*, 168.
(34) Helfand, E.; Tagami, Y. *J. Chem. Phys.* **1972**, *56*, 3592.
(35) Helfand, E.; Sapse, A. *J. Chem. Phys.* **1975**, *62*, 1327.
(36) Vavasour, J. D.; Whitmore, M. D. *Macromolecules* **1993**, *26*, 7070.
(37) Terzis, A. F.; Theodorou, D. N.; Stroeks, A. *Macromolecules* **2000**, *33*, 1385.
(38) Daoulas, K. Ch.; Müller, M. *Adv. Polym. Sci.* **2010**, *224*, 197.
(39) Müller, M. *Macromol. Theory Simul.* **1999**, *8*, 343.
(40) Müller, M. *Phys. Rev. E* **2002**, *65*, 030802.
(41) Schmid, F. *J. Phys: Condens. Matter* **1998**, *10*, 8105.
(42) Fredrickson, G. H.; Ganesan, V.; Drolet, F. *Macromolecules* **2002**, *35*, 16.
(43) Matsen, M. W. *J. Phys: Condens. Matter* **2002**, *14*, 21.
(44) Müller, M.; Schmid, F. *Adv. Polym. Sci.* **2005**, *185*, 1.
(45) Fredrickson, G. H. *The Equilibrium Theory of Inhomogeneous Polymers*: Oxford University Press: Oxford, U.K., 2005.
(46) Müller, M. In *Soft Matter*; Gompper, G., Schick, M., Eds.; Wiley VCH: Weinheim, Germany, 2005; Vol. *1*.
(47) Drolet, F.; Fredrickson, G. H. *Phys. Rev. Lett.* **1999**, *83*, 4317.
(48) Haley, J. C.; Lodge, T. P. *J. Chem. Phys.* **2005**, *122*, 234914.
(49) Schmid, F.; Müller, M. *Macromolecules* **1995**, *28*, 8639.
(50) Jo, W. H.; Lee, S. C. *Macromolecules* **1990**, *23*, 2261.
(51) (a) Tirumala, V. R.; Daga, V.; Bosse, A. W.; Romang, A.; Ilavsky, J.; Lin, E. K.; Watkins, J. J. *Macromolecules* **2008**, *41*, 7978. (b) Tirumala, V. R.; Romang, A.; Agarwal, S.; Lin, E. K.; Watkins, J. J. *Adv. Mater.* **2008**, *20*, 1603.
(52) Kim, S.; Briber, R. M.; Karim, A.; Jones, R. L.; Kim, O. C. *Macromolecules* **2007**, *40*, 4102.

(53) (a) Lin, Z.; Kim, D. H.; Wu, X.; Boosahda, L.; Stone, D.; LaRose, L.; Russell, T. P. *Adv. Mater*. **2002**, *14*, 1373. (b) Kim, S. H.; Misner, M. J.; Xu, T.; Kimura, M.; Russell, T. P. *Adv. Mater*. **2004**, *16*, 226.
(54) Kim, S. H.; Misner, M. J.; Yang, L.; Gang, O.; Ocko, B. M.; Russell, T. P. *Macromolecules* **2006**, *39*, 8473.
(55) Bendejacq, D.; Ponsinet, V.; Joanicot, M.; Loo, Y. L.; Register, R. A. *Macromolecules* **2002**, *35*, 6645.
(56) Xu, R.; Winnik, M. A.; Riess, G.; Chu, B.; Croucher, M. D. *Macromolecules* **1992**, *25*, 644.
(57) Chen, H. Y.; Fredrickson, G. H. *J. Chem. Phys*. **2002**, *116*, 1137.
(58) Meng, D.; Wang, Q. *J. Chem. Phys*. **2007**, *126*, 234902.
(59) Xianfeng, L.; Fustin, C. A.; Lefèvre, N.; Gohy, J. F.; De Feyter, S.; De Baerdemaeker, J.; Eggere, W.; Vankelecom, I. F. J. *J. Mater. Chem*. **2010**, *20*, 4333.